Supporting Information

Liquid-liquid phase separation modifies the dynamic properties of intrinsically disordered proteins

Serafima Guseva[†], Vincent Schnapka[†], Wiktor Adamski, Damien Maurin, R.W.H. Ruigrok, Nicola Salvi, Martin Blackledge*

Institut de Biologie Structurale,

Université Grenoble Alpes-CEA-CNRS

71, Avenue des Martyrs

Grenoble

France

Figure S1

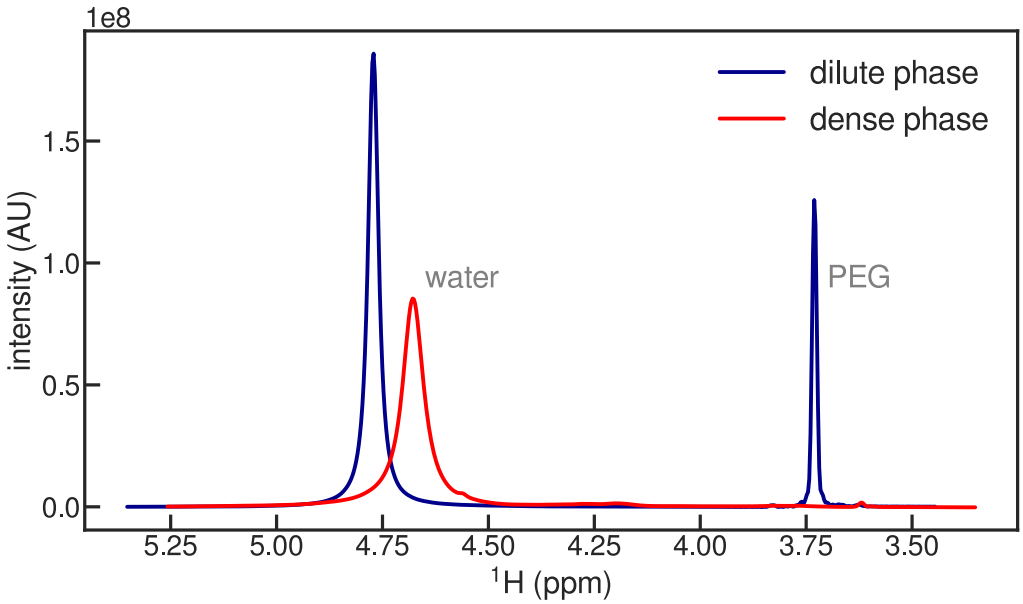

PEG is predominantly localised in the dilute phase of phase-separated N_{TAIL}-PEG mixtures

^{1}H NMR spectra of (a) dense phase, and (b) the coexisting dilute, indicating that PEG is predominantly localised to the dilute phase.

Figure S2

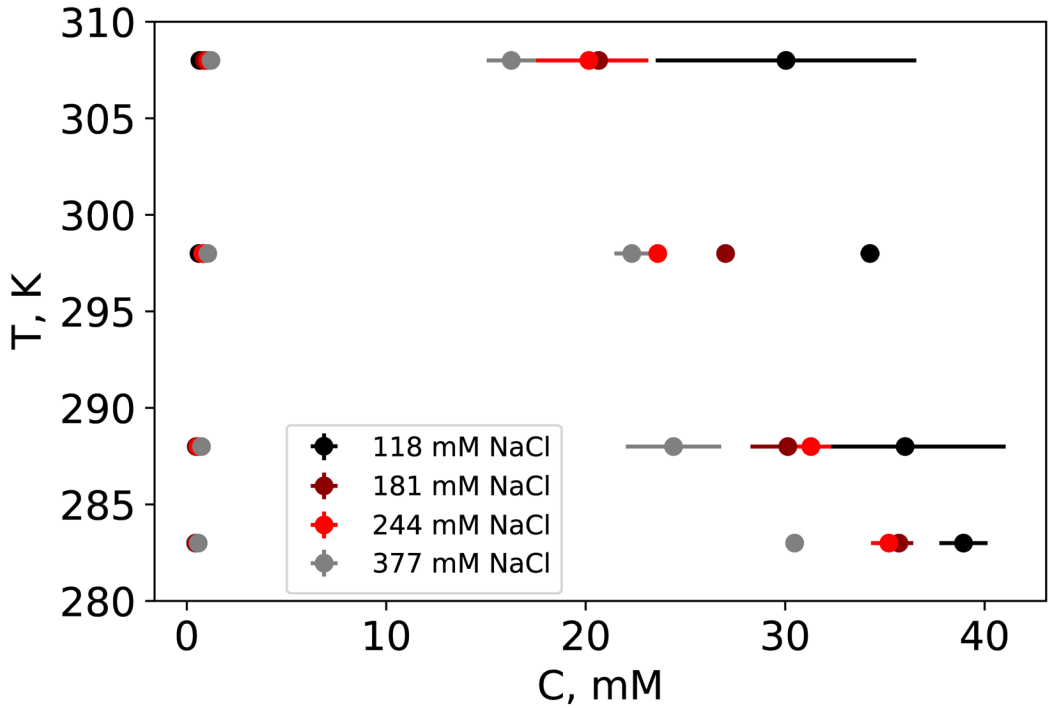

N_{TAIL} phase diagram (molar concentration C) as a dependency on temperature. Different colours correspond to different salt concentrations (black -118, dark red - 181, red - 244 and grey - 377 mM NaCl).

Figure S3A

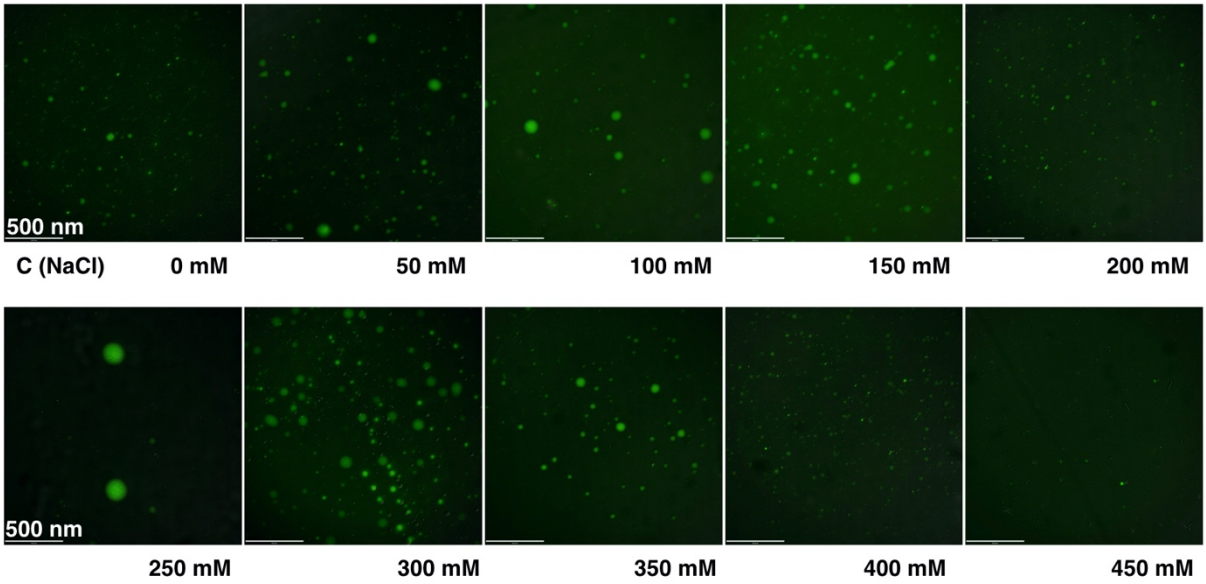

Fluorescent microscopy images of N_{TAIL} droplets taken at different NaCl concentrations.

Figure S3B

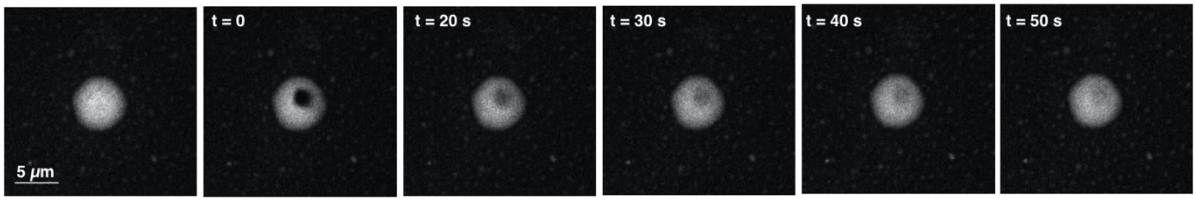

Example of Fluorescence recovery after photobleaching (FRAP) carried out on a single N_{TAIL} droplet (see Methods).

Figure S4

S4A

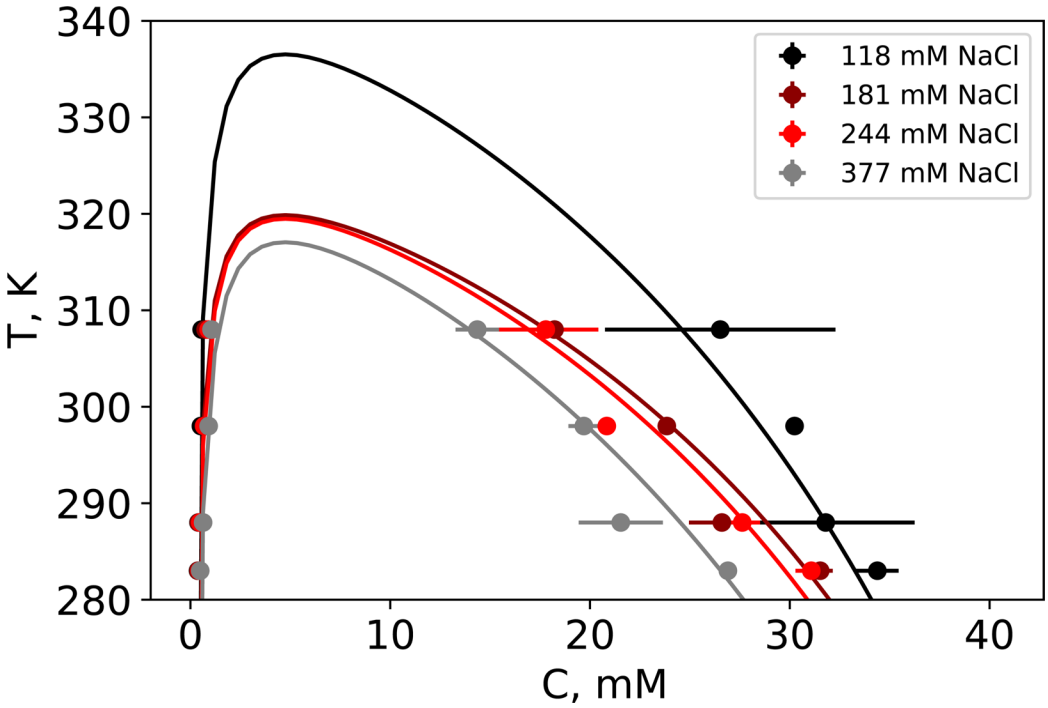

S4B

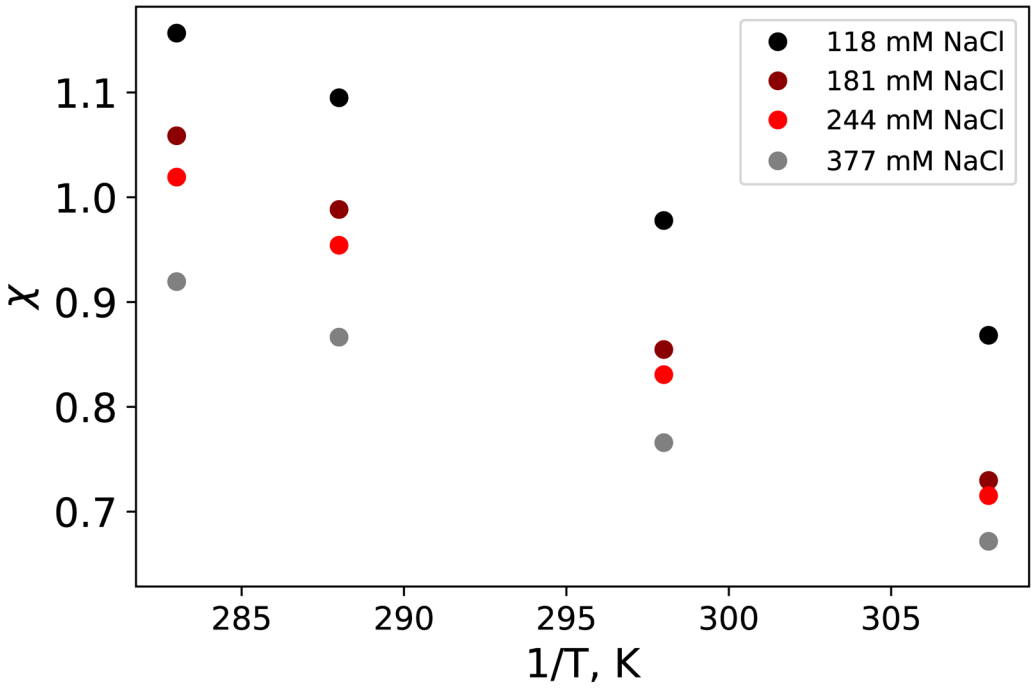

Flory-Huggins model fit of the experimentally determined phase diagram

S4A - Phase diagram calculated from fitting to equation 1.

S4B - Calculated χ parameter for all temperature and salt conditions.

Figure S5

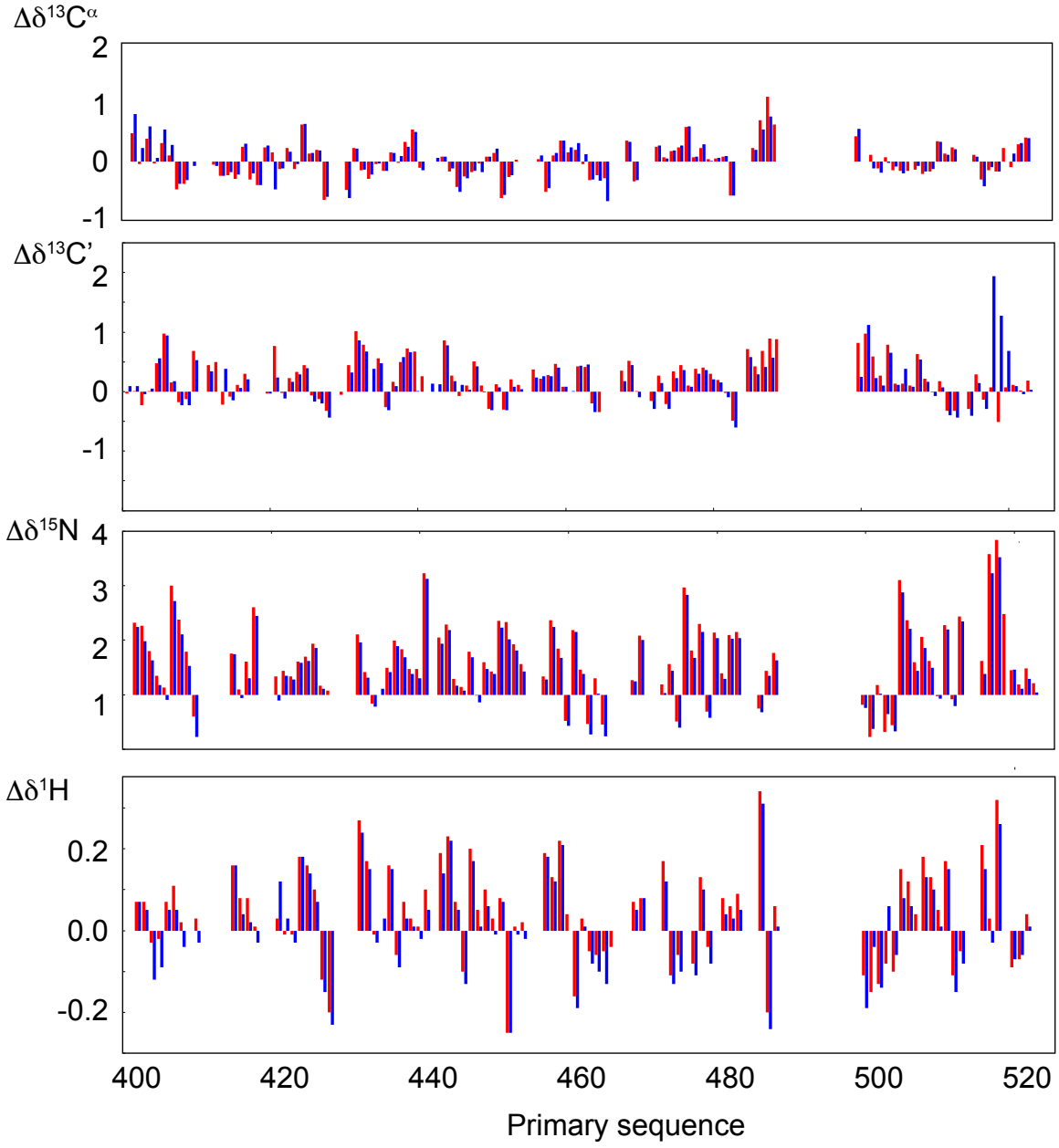

Secondary chemical shifts of N_{TAIL} suggest conserved backbone conformational sampling throughout phase space.

Top to bottom: ^{13}Ca, ^{13}C', ^{15}N and ^{1}H secondary chemical shifts.

Red - N_{TAIL} in the dilute state, blue - N_{TAIL} in the dense phase.

Figure S6

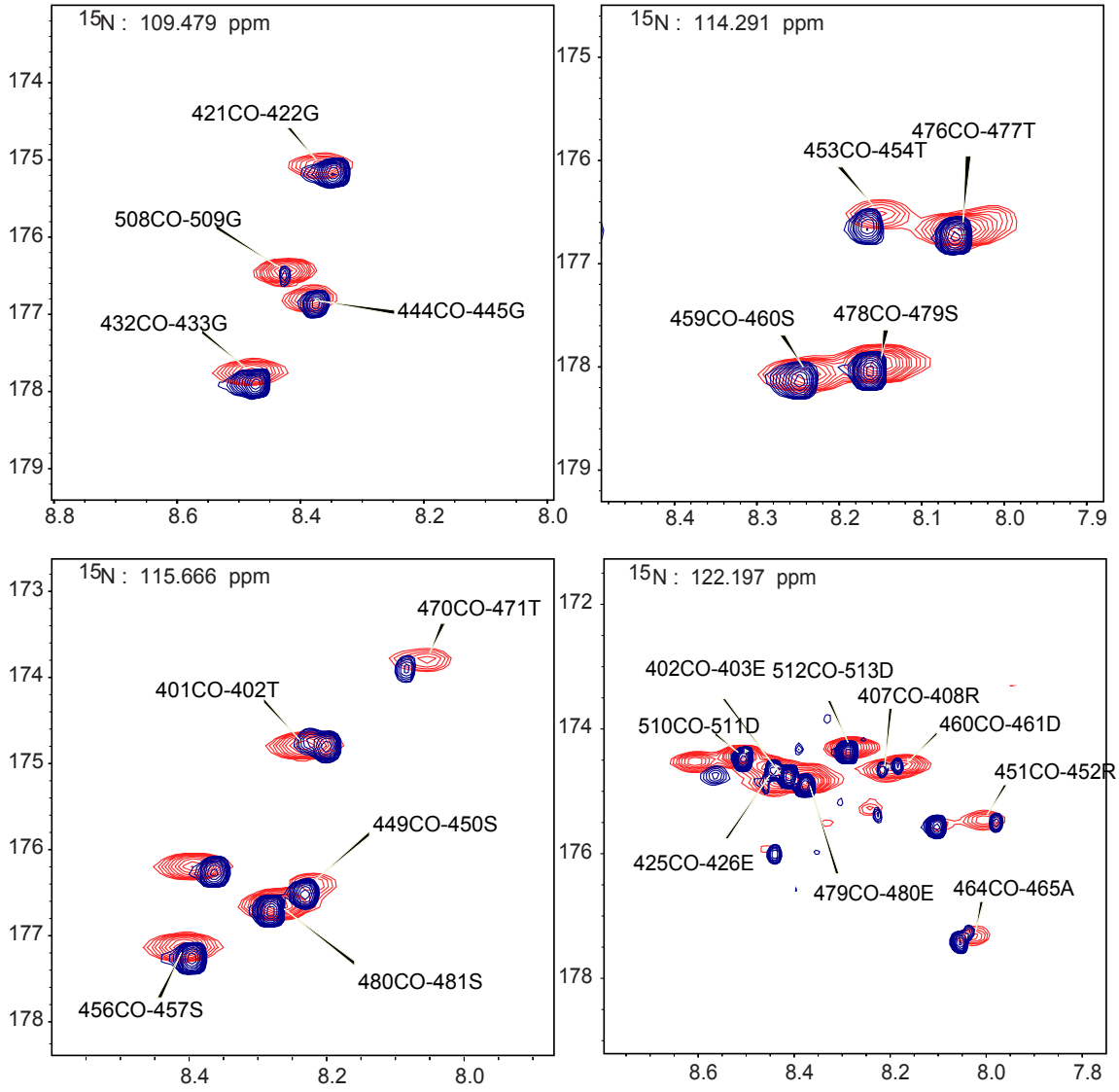

Backbone chemical shifts of N_{TAIL} suggest conserved backbone conformational sampling throughout phase space.

Comparison of ^{15}N planes from triple resonance HNCO experiments on dilute (blue) and dense (red) phase samples showing similarity of ^{N}H-C' correlations under the two conditions.

Figure S7

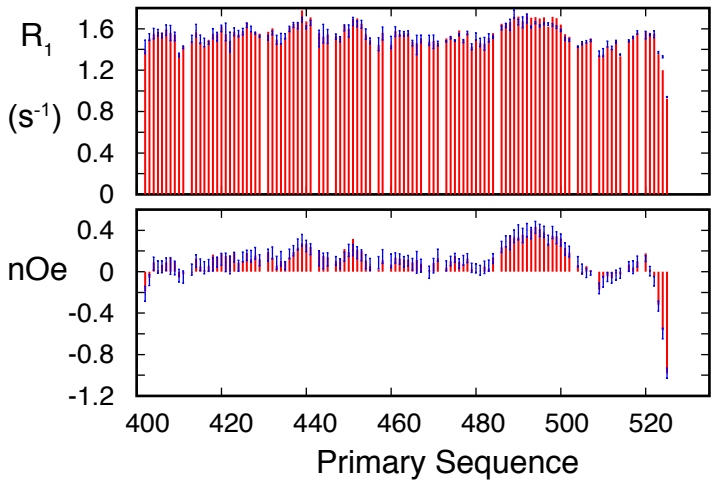

Cross-validation of dynamic model of N_{TAIL} in the dilute phase

Experimental R_1 and heteronuclear ^{1}H-^{15}N nOe measured at 700MHz on the 0g/L (PEG concentration) N_{TAIL} sample in the dilute phase (blue), compared to values back-calculated from the dynamic model-free analysis (red bars) of data measured at 600 and 850 MHz at 0, 37.5 and 75g/L PEG10000). Rmsd values are within the mean experimental error for both R_1 (0.033 compared to 0.0319) and heteronuclear ^{1}H-^{15}N nOe (0.035 compared to 0.042).

Figure S8

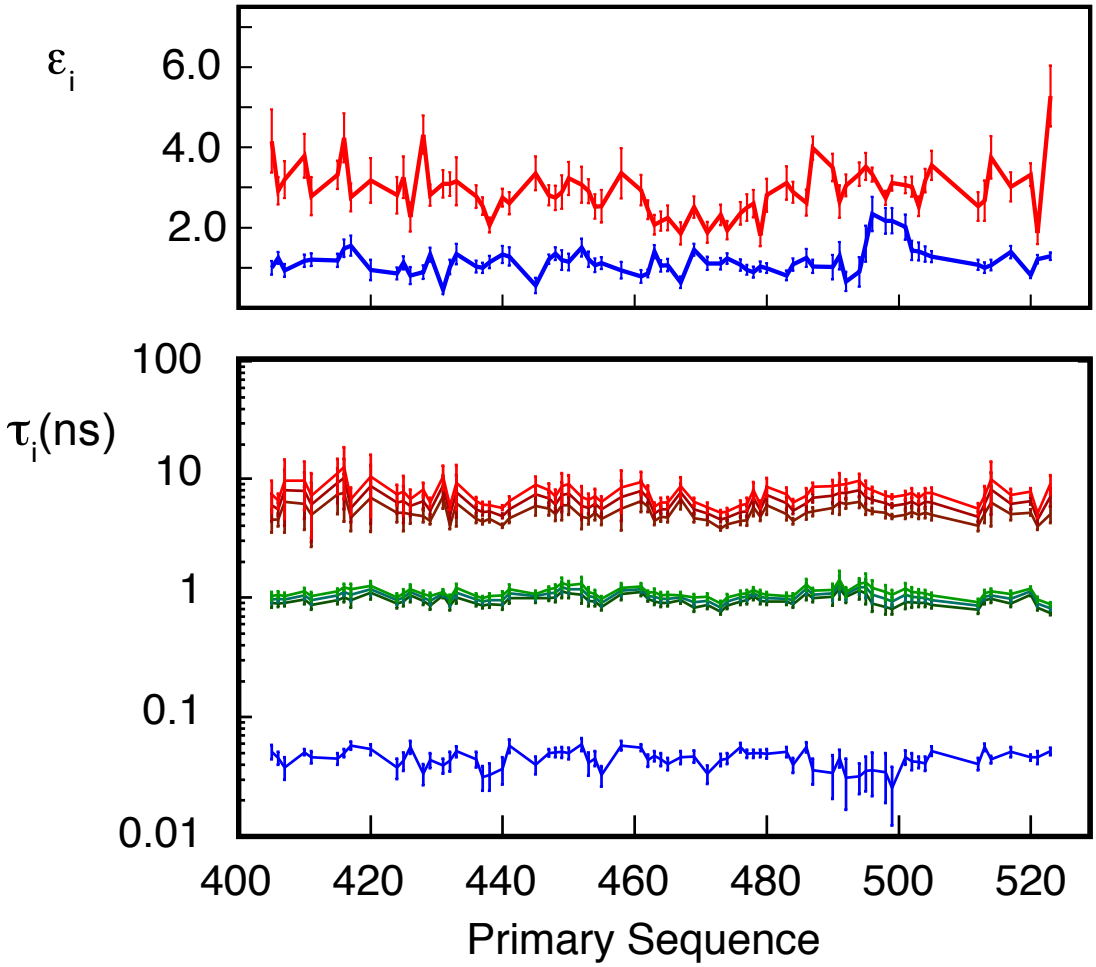

Model-free analysis of dynamic behaviour of N_{TAIL} as a function of viscosity

Top – Residue-specific viscosity coefficients for the intermediate (blue) and slow (red) dynamics modes.

Bottom – Residue-specific correlation times of segmental backbone motions (τ_3)- 0 g/L (dark red), 37.5 g/L (red) and 75 g/L PEG10000 (light red), intermediate, backbone motions (τ_2) - 0 g/L (dark green), 37.5 g/L (green) and 75 g/L PEG10000 (light green) and fast motions (τ_1) (blue)

Figure S9

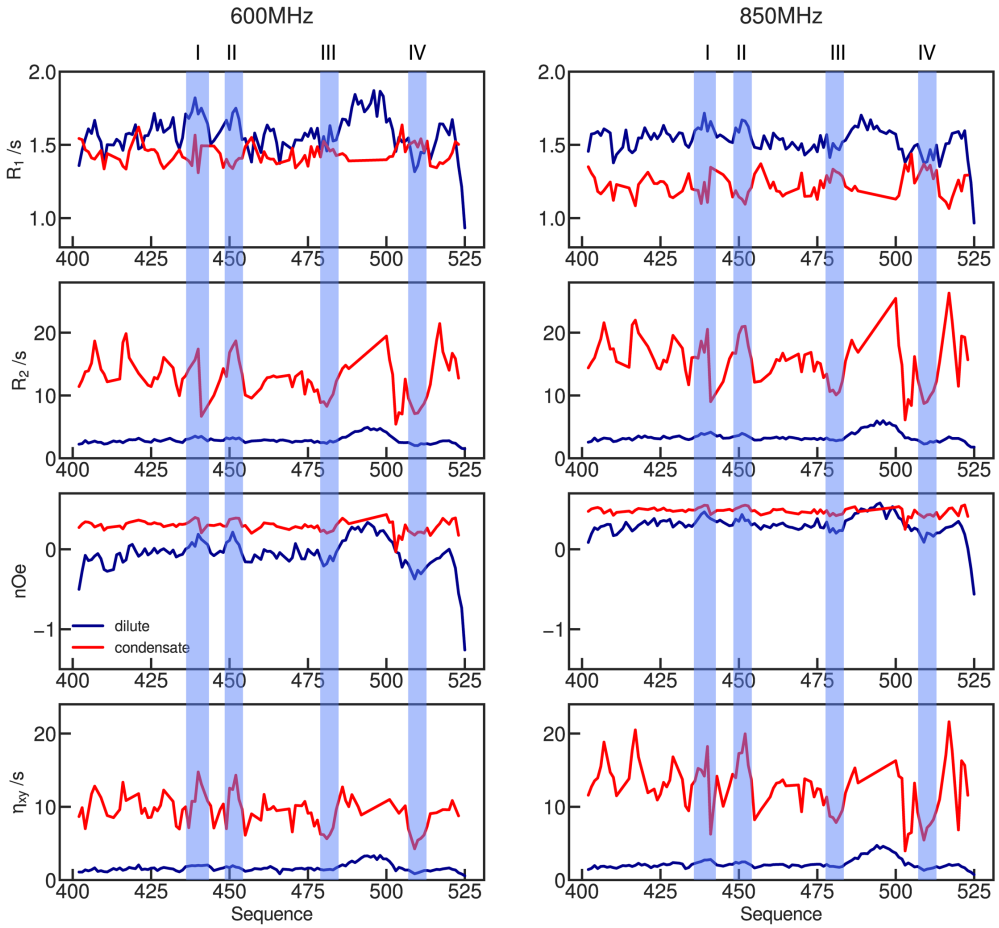

Identification of regions of N_{TAIL} exhibiting specific dynamic behaviour

Figure 4 of the manuscript is reproduced highlighting regions ^{438}RRVK^{441} (I) and ^{449}ESYRE^{453} (II), both exhibiting elevated transverse relaxation rates in both dilute and dense phases, and ^{487}TASESS^{492} (III) and ^{509}GSDT^{512} (IV) that clearly exhibit higher flexibility

Figure S10

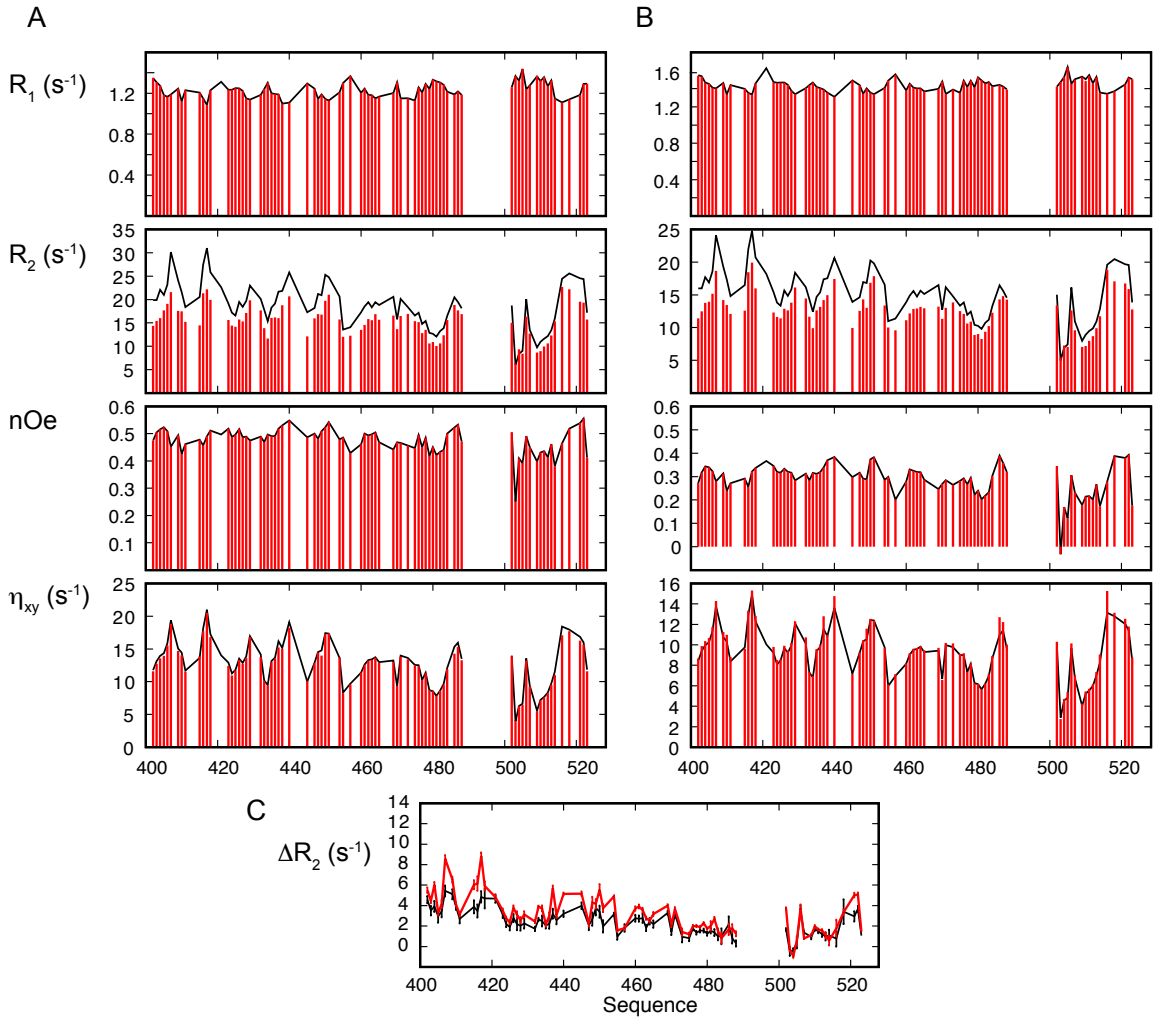

Reproduction of experimental data by model-free analysis of data from the dense phase

88 experimental relaxation rates (black lines) were fitted to equation 7. 5 parameters were optimized ($\tau_1, \tau_2, \tau_3, A_2$ and A_3) by fitting to experimental (black) R_1, η_{xy} and heteronuclear $\{^1H\}$-^{15}N nOe at two magnetic field strengths (A-850 and B-600 MHz). Calculated values are shown as red bars. C - R_2 values were back-calculated from this model-free analysis, and compared to experimental values ($\Delta R_2 = R_{2,calc} - R_{2,exp}$) (red 850MHz, black – 600 MHz).

Figure S11

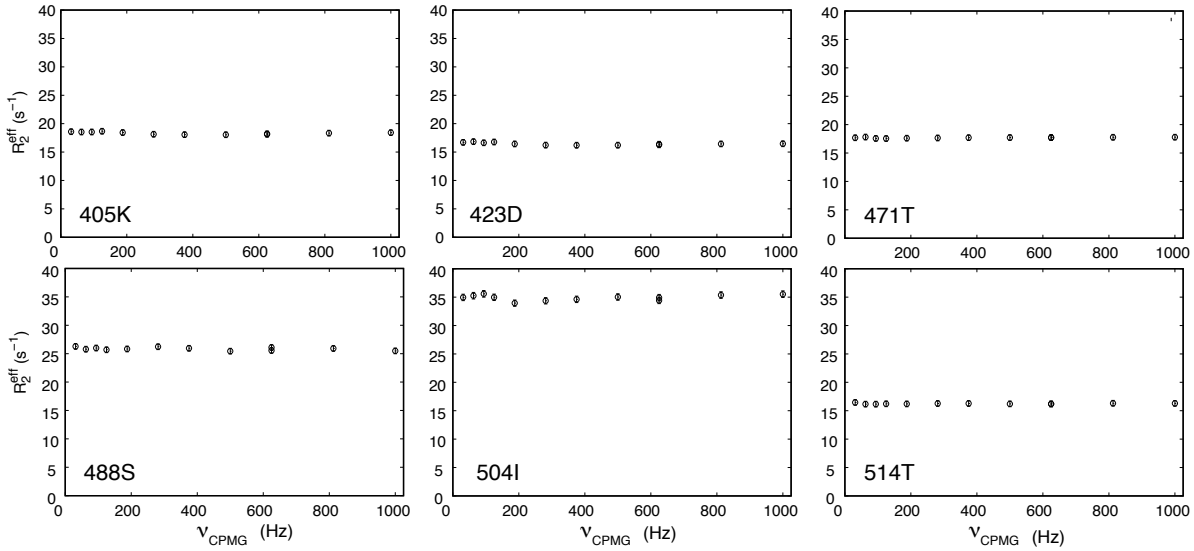

Relaxation dispersion CPMG experiments carried on the N_{TAIL} in the dense phase

Relaxation dispersion CPMG was carried out at 950 MHz in the dense phase, revealing no evidence for significant chemical shift exchange, as illustrated from 6 randomly selected amino acids along the primary sequence.

Figure S12

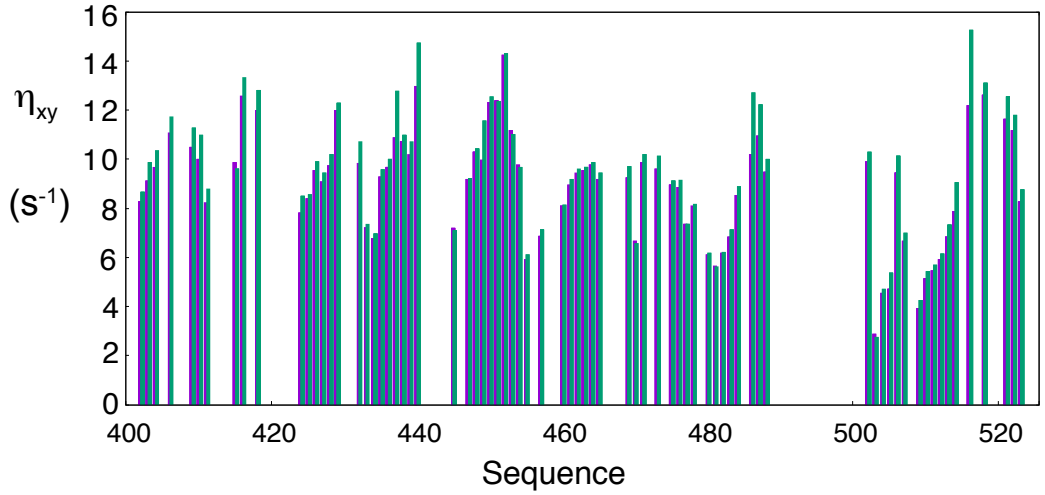

Reproduction of experimental data by model-free analysis of data from the dense phase

Experimental η_{xy} rates (blue bars) that were removed from the fit equation 7 and predicted from the fit of R_1, and heteronuclear $\{^1H\}$-^{15}N nOe at 600 MHz and R_1, η_{xy} and heteronuclear $\{^1H\}$-^{15}N nOe at 850MHz. Calculated values are shown as green bars.

Figure S13

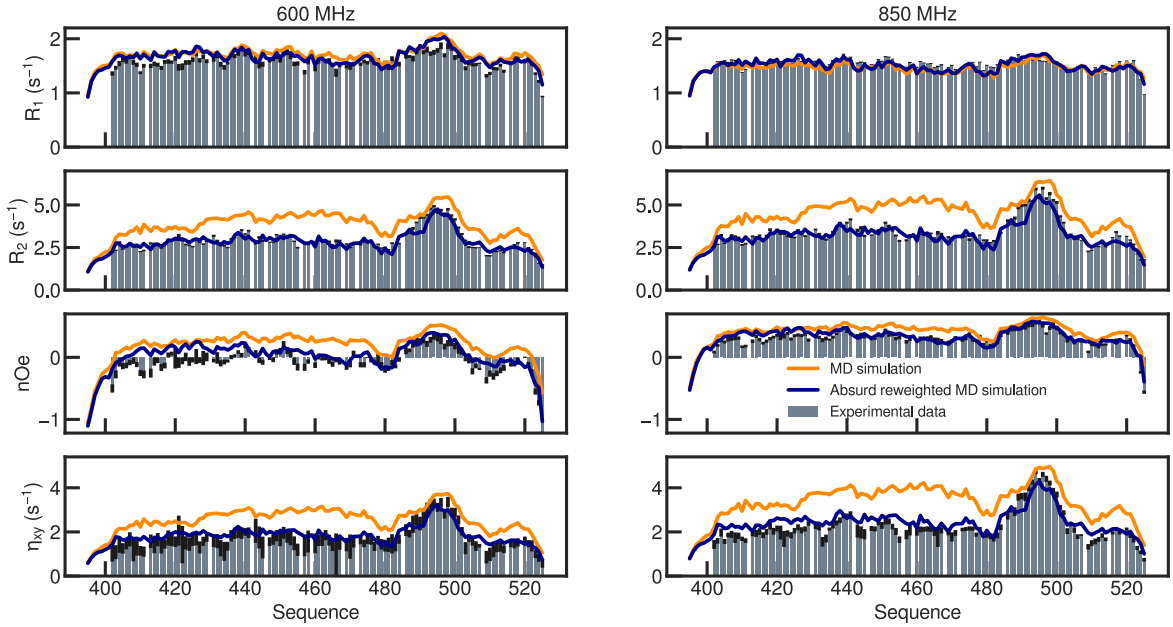

Reproduction of experimental relaxation rates using ABSURD ensemble trajectory analysis

MD simulation of were performed with CHARMM36m (C36m) in combination with the TIP4P/2005 (t4p2005) water model. 30 trajectories of 200ns were calculated and analyzed. Predicted rates (orange) failed to accurately reproduce experimental rates (bars), especially those sensitive to J(0). The ABSURD genetic algorithm targetting R_2 at 850MHz selects the combination of trajectories that best reproduce this rate. Improvements in the agreement with all other experimental data is also observed (blue lines), indicating a better representation of the dynamic ensemble.

Figure S14

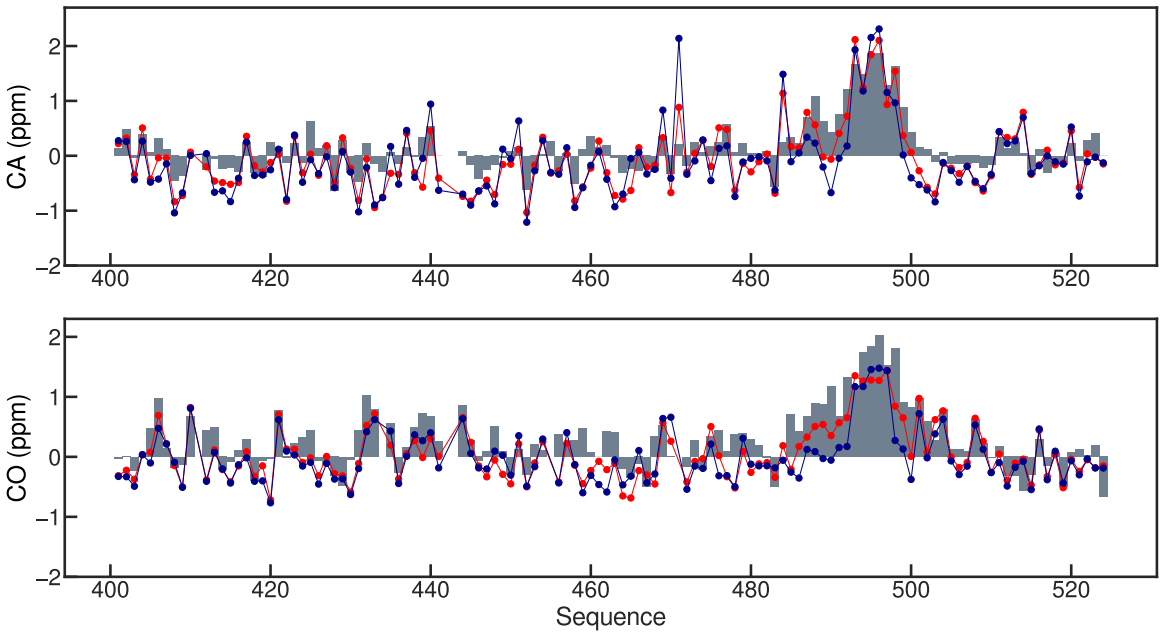

Reproduction of experimental chemical shifts using ABSURD ensemble trajectory analysis and MD simulations of highly concentrated N_{TAIL}

Chemical shifts prediction derived from MD simulations of dilute (ABSURD ensemble of trajectories - blue), 20mM N_{TAIL} concentration (red) compared with experimental data from the dilute phase (grey bars).

Figure S15

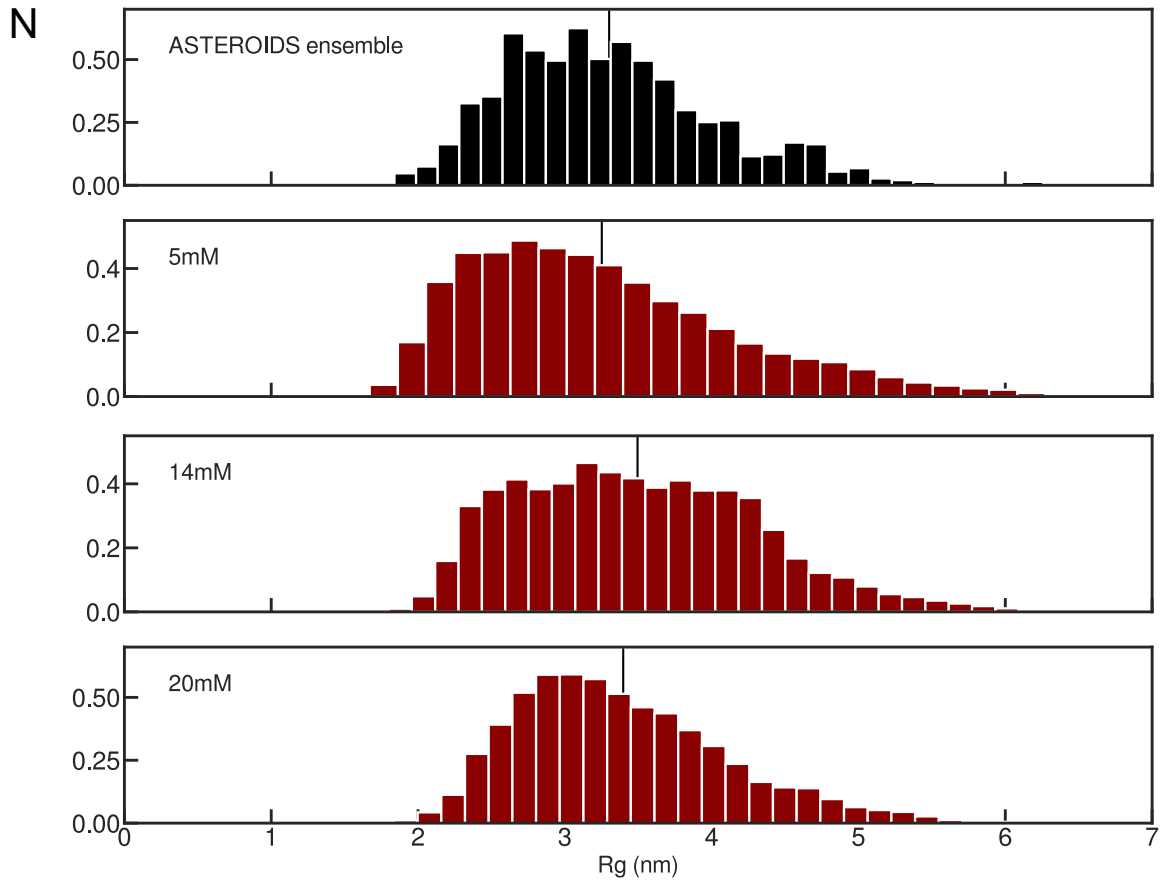

Distribution of radii of gyration of the ASTEROIDS ensemble and MD simulations of highly concentrated N_{TAIL}

Radii of gyration were averaged over 100 conformers in the ASTEROIDS ensemble, and over 200ns and 125, 125 and 343 copies of the protein for the self-crowding simulations (5, 14 and 20mM respectively).

Figure S16

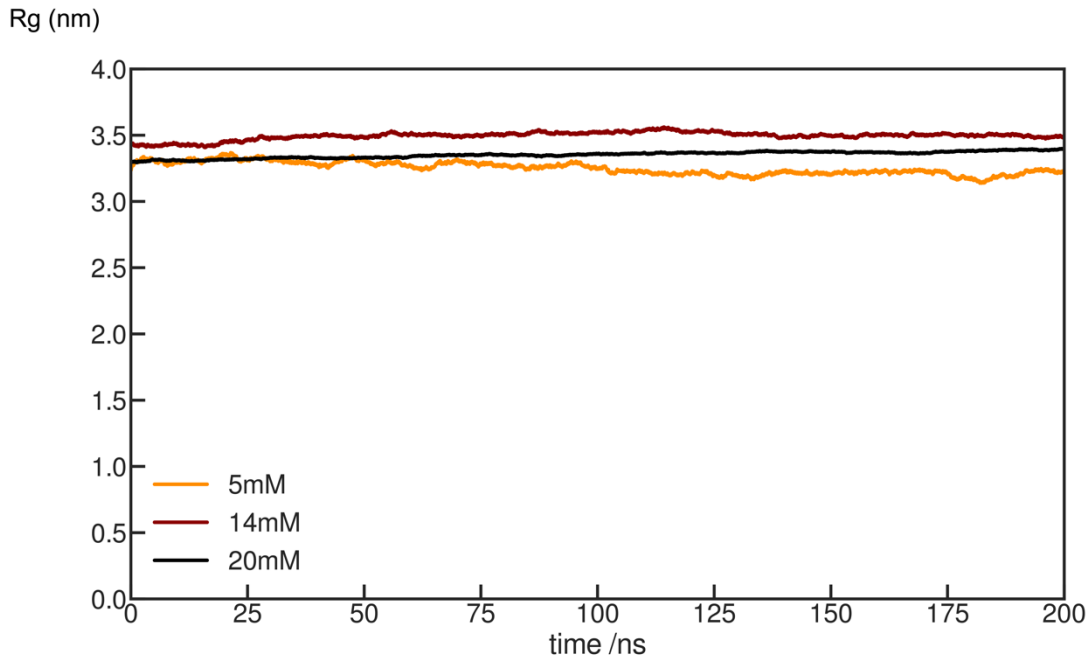

Evolution of average radii of gyration of the MD simulations of highly concentrated N_{TAIL}

Radii of gyration were averaged over 125, 125 and 343 copies of the protein for the self-crowding simulations (5, 14 and 20mM respectively).

Figure S17

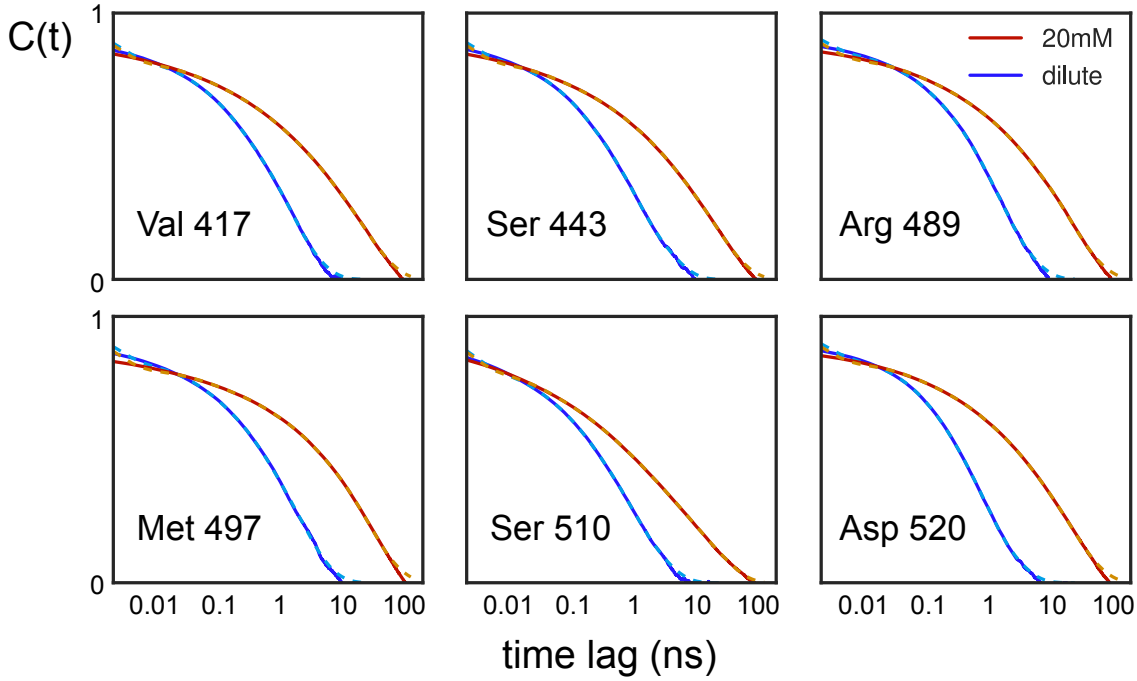

Comparison of autocorrelation functions calculated from dilute and concentrated phase simulations

Solid lines show correlation functions calculated from the ABSURD-derived ensemble of trajectories describing the dilute phase (blue) and the 20mM N_{TAIL} box (red), in this case the correlation function is averaged over 343 copies. Orange and light blue dashed lines show the fit to the correlation functions used to calculate the relaxation rates. Correlation functions (417, 443, 489, 497, 510 and 520) were randomly selected along the primary sequence.

Figure S18

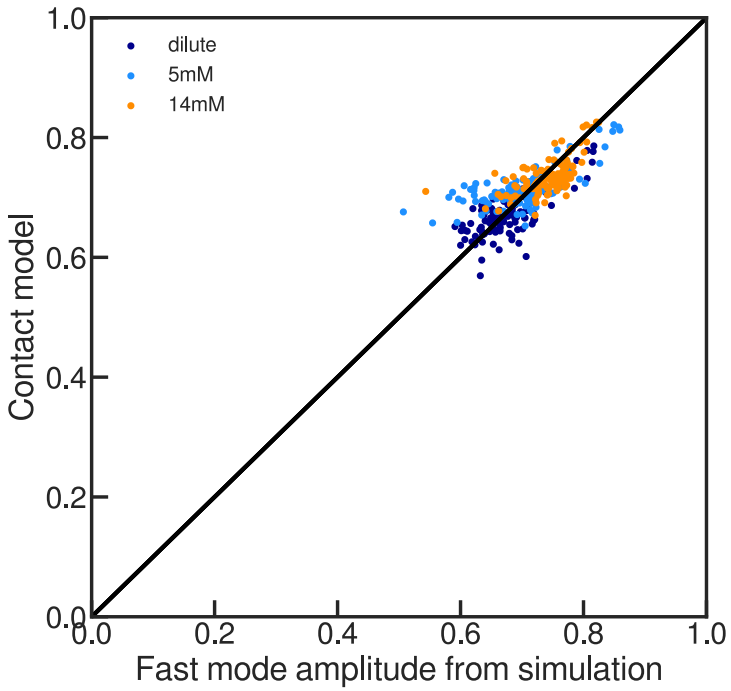

Correlation of amplitudes of motions calculated from the contact model (see methods) and derived from model free analysis of simulated relaxation rates.